International Journal of Nanoelectronics and Materials
IJNeaM
ISSN 198-5761 | E-ISSN 2232-1535

Physical Investigations of GaN/Porous Silicon at Different Laser Wavelengths

Rusul S. Rashed[a], Makram A. Fakhri[a,*], Ali A. Alwahib[a], Motahher A. Qaeed[b] and Subash C. B. Gopinath[c,d,e]

[a]*Laser and Optoelectronic Department, University of Technology-Iraq, Baghdad, Iraq.*
[b]*Physics Department, Faculty of Science, University of Jeddah, Jeddah, Saudi Arabia.*
[c]*Institute of Nano Electronic Engineering, Universiti Malaysia Perlis (UniMAP), 01000 Kangar, Perlis, Malaysia.*
[d]*Faculty of Chemical Engineering & Technology, Universiti Malaysia Perlis (UniMAP), 02600 Arau, Perlis, Malaysia.*
[e]*Micro System Technology, Centre of Excellence (CoE), Universiti Malaysia Perlis (UniMAP), Pauh Campus, 02600 Arau, Perlis, Malaysia.*
**Corresponding author. E-mail: mokaram_76@yahoo.com, & makram.a.fakhri@uotechnology.edu.iq*

ABSTRACT

In this study, we prepared PSi using the laser-assisted electrochemical etching method and deposited Gallium nitride (GaN) on the PSi substrate using the pulsed laser technique at different pulsed laser wavelengths (1064, 532, and 355 nm). We investigated the optical, structural, topographical, and morphological properties of Gallium Nitride on the substrate PSi by various pulsed laser wavelengths. The X-Ray Diffraction (XRD) analysis revealed that gallium nitride on PSi was polycrystalline and hexagonal, cubic structural at 532 nm, with a high peak intensity and crystallite size at 2θ=36.96°and 57.80 related to (101) and (110) planes, respectively, while the c-GaN phase is observed at 2θ = 25.43 degrees and is reflected from the (200) plane. PL shows two emission peaks were observed for the GaN film (430,345,413 nm) and the PSi substrate (867,891,876 nm), and the energy gap increased as the wavelength decreased. The field emission scanning electron microscopy (FESEM) pictures revealed that the synthetic sample had an average size of 24.45, 23.91, and 21.30 nm, and the nanoparticles appeared spherical and similar to cauliflower. The atomic force microscopy (AFM) results showed that the average roughness was 7.62, 10.64, and 13.62 nm, respectively, and it was observed the root mean square increased as a result of the uniform distribution of high-quality crystals and the excellent quality of the crystal structure. The UV-Visible (UV) results showed that the transmission decreased with a decrease in wavelength, and the absorption was inversely proportional to the transmission.

Keywords: *Gallium Nitrite (GaN), Poros Silicon (PSi), Pulse Laser Deposition (PLD), Photoelectrochemical etching, Physical properties*

1. INTRODUCTION

The physical characteristics of gallium nitride (GaN), which include strong thermal conductivity, a broad and direct band gap, and low compressibility, have attracted a lot of attention recently. It is an appealing material for use in optical devices because of these qualities [1–4]. GaN technology can operate under challenging conditions [5, 6]. GaN is a very strong and stable semiconductor material with a broad bandgap of 3.4 eV, which makes it perfect for many applications, including sensors [7-9], field effect transistors (FETs) [10–12], and light-emitting diodes (LEDs) [13–15]. Additionally, because of its excellent thermal conductivity and large heat capacity, it is appropriate for high-power electrical equipment. Due to their potential application in solid-state lighting, the optical characteristics of GaN nanostructures have also drawn a lot of attention [16–18]. GaN is an overall promising material for a variety of technological applications thanks to its unique features. It is a promising contender for optoelectronic devices because of the straight bandgap. Additionally, new possibilities in chemical and biochemical sensing are made possible by the electronic structure's sensitivity to the physical and chemical characteristics of the GaN surface [19–22].

Despite being widely available and reasonably priced, silicon is inadequate for electronic systems that need to function in harsh conditions or demand high power throughput because to restrictions caused by its extremely modest bandgap (1.1 eV) [23-25]. As a result, there is an increasing need for substitute semiconductors that can satisfy these needs. One such semiconductor with characteristics that enable it to work in these circumstances is GaN [26-29]. It is more suitable for high-power and high-temperature applications due to its larger bandgap and greater breakdown voltage than silicon. As a result, it has drawn interest as a possible silicon substitute in several electrical devices in recent years [30-32].

GaN thin films are being made using both physical and chemical deposition by vapors (CVD) techniques, including the epitaxy of the molecular beam, low-pressure, pressure atmospheric, metal-organic, plasma enhanced, and the hot-wire, also the deposition using vapor techniques, like laser deposition by pulsed (PLD), are all being used to deposit GaN Nano-films [33-35].

Tunable Porosity: The optical and electrical properties of porous silicon can be precisely controlled by fabricating it with a broad variety of porosities, pore sizes, and pore distributions. It is adaptable to various optoelectronic device designs and operations thanks to its tunability. High Surface Area: Due to silicon's porous structure, which significantly expands its surface area, it may interact with

light more effectively and have higher sensitivity in sensor applications. Additionally, the effective charge transfer in solar cells and photodetectors is made possible by this large surface area. Porous silicon has distinct optical characteristics[36-38]. Because of its unique characteristics, such Optical Properties: By modifying the pore structure and surface chemistry, porous silicon can display a variety of unique optical properties, such as photoluminescence. These optical characteristics are utilised in optical sensors for imaging and detection applications as well as in light-emitting devices like LEDs. Compatibility with Silicon Technology: By utilising the current infrastructure and knowledge in silicon technology, porous silicon can be easily integrated with traditional silicon-based fabrication techniques. The creation of hybrid devices and integrated optoelectronic systems is made possible by this compatibility. [39-41]. Biocompatibility: Because porous silicon is biocompatible, it can be used in biosensors. Its optical and electrical properties, along with its biocompatibility, present prospects for improved medical diagnostics and treatments. All things considered, porous silicon's remarkable qualities make it an extremely promising material for a variety of optoelectronic applications, spurring continuous research and development efforts to realise its full potential in a number of disciplines. The purpose of this study was to examine the use of a solid-state Nd:YAG pulsed laser in the Pulsed Laser Deposition (PLD) process to deposit a Nan-GaN layer onto PSi substrates while taking into account different preparation factors. The primary focus of this work was the effect of different PLD wavelengths on the optical (PL, XRD, and EDS), structural (XRD, and EDS), morphological (AFM, FESEM), and performance features of the GaN structure on a PSi substrate.

2. METHODOLOGY

2.1 PSi Substrate Preparation

By using the diode laser-assisted photoelectrochemical etching approach, silicon wafers (n-type) with a single side polished Mon crystalline, 500m thick, 0.001-0.005 Ω/cm electrical resistance, and (111) orientations were used to create PSi substrates at room temperature. The digital multimeter (China, Victor Inc., VC97), the wavelength is 660 nm, the power is 100 mw (China, Tongtool Inc.), and the electrolyte solution is 48% hydrofluoric acid (German, Thomas Baker) and 99.9% ethanol (German, Honeywell Corporation). The DC power supply ranges from 0 to 30V (China, Jiuyuan). The silicon wafers were divided into tiny fragments, each measuring one. After using ethanol to clean these parts, we dried them. Next A synthetic etching electrolyte solution made of a combination of concentrated hydrofluoric acid (48%) and ethanol (99.9%) was used to submerge the A silicon wafer.The wafer was exposed to a current density of 10 mA/ for ten minutes while it was submerged. We produced PSi substrate by utilising a 100-mW laser diode with precise control over the intensity and spot size, we can optimise the formation of a porous structure on a silicon substrate when using hydrofluoric acid for etching. By adjusting the intensity (I) and duration of the laser exposure, you can control the depth and density of the porous structure. Higher intensities or longer exposure times can create deeper and denser porous layers. The intensity of the laser spot can be calculated using a law:

Intensity (I) = Laser Power (P) / Beam Area (A).

Additionally, we employed silicon as the anode and a fluorine cell with 95% pure platinum electrodes (from Turkey) as the cathode during the process, as shown in Figure 1. Illustrates in Table 1 the characteristics of the laser-assisted top-down photo electrochemical etching technique used to make PSi.

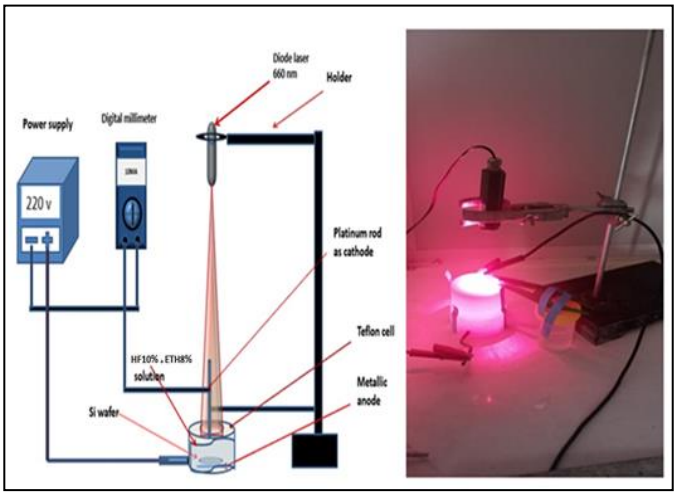

Figure 1. A schematic of the photo electrochemical etching technique used to create PSi substrates.

Table 1 Lists of process parameters for electrochemical etching induced by lase

Etching time (Minte)	Concentration of HF	Current density (mA/cm²)	Wavelength of the laser (mw)	Power of the induced laser (mw)
10	48%	10	600	100

The PSi was carefully put in a Teflon cell and sealed, following which the electrolyte was added and the power supply was turned on. The current density was measured using a multimeter and controlled by adjusting the voltage of the power supply to maintain a fixed current of 10 mA/s (as the current changes during the process). The moment the power supply was turned on, the timer was set to begin. Figure 2 shows images of the prepared PSi, taken under natural light and near UV light, respectively.

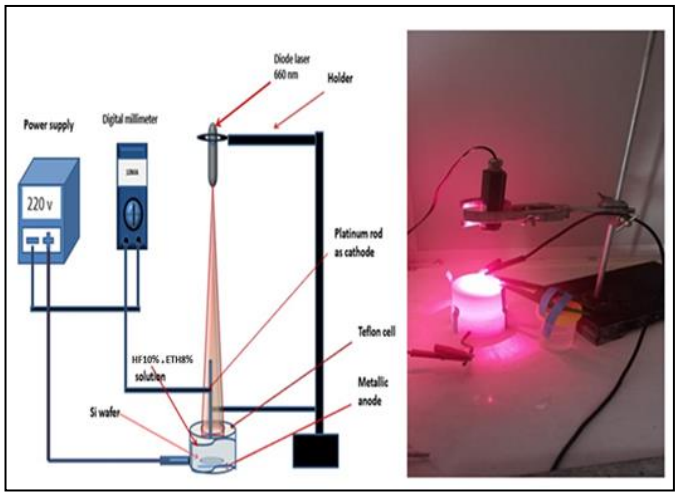

Figure 2. Porous silicon prepared, a) under natural light, b) under near UV light.

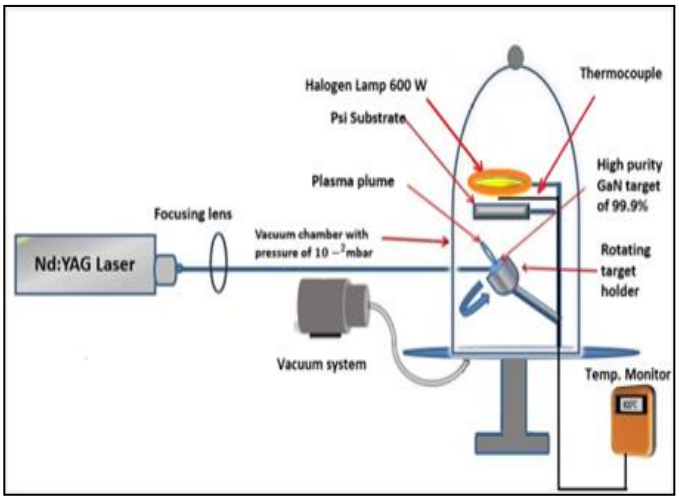

Figure 3. The schematic design for the PLD process using GaN on a PSi substrate at several wavelengths (1064, 532, and 355 nm).

2.2 GaN Target Preparation

The purity of the PLD target, which is made of GaN, is 99.9%, and it was purchased from Technologically University. The diameter of the target is 2.5 cm, and its thickness measures 5 mm.

2.3 GaN Films are Prepared by PLD

The PLD setup typically includes a pulse laser, avariac, thermometer, and a container that is completely insulated to help stop any gas from starting to leak out. There are two openings that work on the air flow and are governed through tubes; one of these openings is for the vacuum pump, and the other is for the insoluble gas. This container contains a halogen lamp 600 w, a platform on which the substrate is fixed (and which is spaced from the target by 2 to 10 cm), a spinning stand on which the material is fixed, and power connections. Figure 3 depicts the PLD system applied to this work. The substance is removed when the high-energy pulsed laser beam concentrates on it. The target is mounted on the platform; it spins to avoid colliding in the same place, and to ensure the best removal, the laser impacts the target at a 45-degree angle. [42-44]. At the beginning of the laser pulse, a significant vapor layer will appear in front of the target. This vapor will absorb energy, which will lead to high temperature and pressure, and this will lead to partial ionization. Increasing the rise pressure causes this layer to expand, forming a cloud known as the plasma column. Throughout smoke formation, the internal ionization and heating energies of the molecules are converted into kinetic energy [45-47]. In this work, Nd: YAG lasers were utilized at different wavelengths (1064nm, 532 nm, and 355 nm) to determine the ideal wavelength to create GaN films with excellent homogeneity and regular distribution of the particles, as shown in figure 2. Parameters used in PLD are shown in Table 2.

Table 2 Lists of PLD parameters for using GaN on a Psi substrate

Parameters of the pulsed Laser	The values
Wavelengths of the pulsed Laser	1064nm,532nm,355nm
Energy of the pulsed Laser	2000 mJ
Duration of the pulse	10 ns
Frequency of the pulsed Laser	220 v
Substrate	PSi, quartz
Substrate temperature	300°C

Following the completion of the deposition process, every PSi substrate that has GaN coated on it is put through screening procedures to find the best outcome for various wavelengths from the United States of America (TT-2 Workshop Company). X-ray diffraction (XRD) from Japan (XRD6000 Shimadzu Company) with copper radiation of 1.54060 was used to assess the structural properties. The topographical features were evaluated using high-resolution microscopy (AFM), and the morphological attributes were evaluated using field emission scanning electron microscopy (FESEM) from Germany (ZEISS Company). The Perkin Elmer Company in the USA provided photoluminescence (PL) for testing the spectroscopic properties.

3. RESULT AND DISCUSSION

3.1. Crystalline Characteristics (XRD)

Figure 4 shows the XRD pattern that illustrates the crystalline properties of the PSi substrate. The X-ray diffraction (XRD) pattern for the sample was collected within the 2θ range of 26° to 30°, and no diffraction signals were detected beyond 2θ = 30°. This indicates that the crystal structure of the sample did not exhibit any reflections at angles greater than 30°. From the XRD pattern, one distinct peak is observed at 2θ angles of 28.4° which are reflected from (200) crystal planes of the PSi substrate by comparing the observed peaks in the diffraction pattern with the known peaks of The crystal

structure of silicon may be determined and verified using the standard silicon (JCPDS card 27-1402). We provided the structural details of the substrate of the PSi described in Table 3. By using the Scherrer equation to calculate the size of the crystals (D) [48].

$$D = K\lambda / \beta \cos\theta \quad (1)$$

Where:
β: full width half maximum of XRD pattern, K (constant Scherer):0.9, λ is the x-ray wavelength, θ: is Bragg's angle in degree.

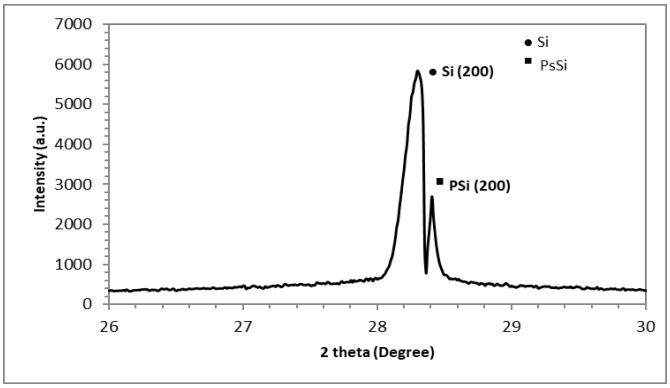

Figure 4. The prepared PSi substrate's XRD pattern.

Table 3 Lists of the PSi substrate XRD properties

Orientation of GaN (hkl)	Angle of the diffraction in Degree	FWHM	The size of Crystallite (D) in nm
200	28.4	0.5	17.17

Figure 5 represents the X-ray diffraction patterns of GaN applied on a PSi substrate at various wavelengths of 1064, 532, and 355 nm, with a constant energy of 2000 mJ and a temperature of 300 C°. Diffraction signals are seen in the X-ray diffraction pattern between 20 and 70 degrees of 2θ, but no peaks are visible after 70 degrees. X-ray analyses reveal a polycrystalline structure due to the different peaks at diffraction patterns (200), (101), and (110)[49]. In the figure 5 (a, b, c) at 1064 nm,532nm,355nm, peaks corresponding to both the h-GaN and c-GaN phases are observed, h-GaN nanoparticles are observed at 2θ = 36.88 and 57.80 degrees, corresponding to the (101) and (110) planes, respectively. The results are identical to the card number (JCPDS card No 50-0792). while the c-GaN phase is observed at 2θ = 25.43 degrees and is reflected from the (200) plane, according to [49], as seen in Table 4. The crystallographic texture was prominent on the (101) plane. The GaN film quality and surface morphology were improved as a result of the high peak intensity at 532 nm. Using Debye-Scherrer's formula (2), the average grain size has been determined from the XRD pattern [50].

$$G.S = 0.9\,\lambda / \beta \cos\theta \quad (2)$$

λ is the wavelength of the X-rays, β is the full width at half maximum (FWHM). θ: is Bragg's angle in degree.

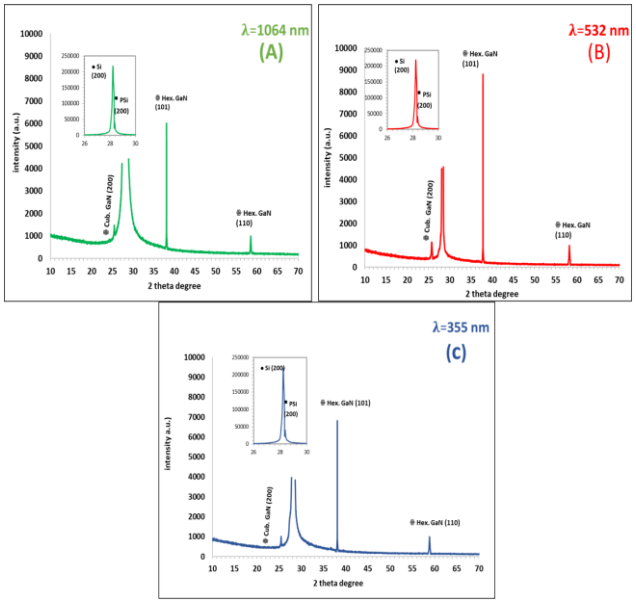

Figure 5. The XRD patterns of the produced GaN/PSi at several laser wavelengths, including 1064 nm, 532 nm, and 355 nm.

Table 4 Lists of the XRD properties of GaN/PSi that were created using various laser wavelengths

Wavelengths of pulsed Laser (nm)	Orientations of GaN (hkl)	The angle of diffraction in (degree)	FWHM	Crystallite size (D) (nm)
1064	200	25.95	0.37	22.54
	101	36.96	0.44	19.33
	110	57.80	0.42	20.25
532	200	25.95	0.46	18.22
	101	36.96	0.36	22.89
	110	57.80	0.52	16.34
355	200	25.95	0.53	15.54
	101	36.96	0.36	22.56
	110	57.80	0.65	12.66

3.2 AFM Surface Topography

Figure 6 displays the PSi substrate produced by the electrochemical etching induced by laser was examined using surface topography analysis employing 3D AFM. Oval-shaped particles with varied heights and a vertical orientation were visible on the surface of the PSi. Table 5 lists the AFM settings for the substrate of PSi.

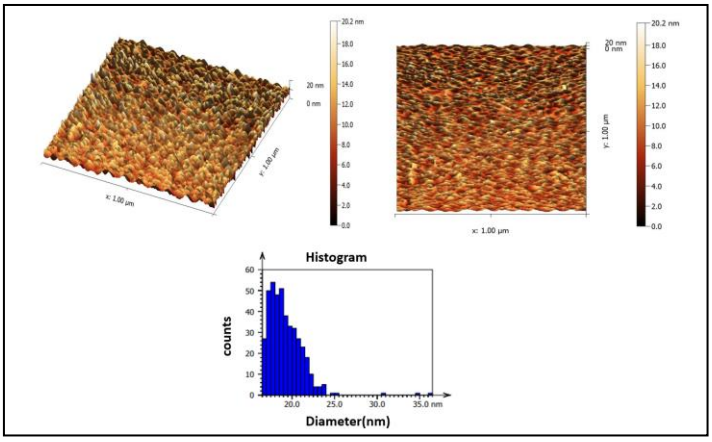

Figure 6. A 3D image of the AFM of a PSi substrate created using an Electrochemical etching induced by laser.

Table 5 Lists of the PSi substrate' produced AFM parameters

Applied Current Density in mA/cm^2	Root-mean-square in nm	Ssurface roughness "Average" in nm
10	2.72	9.49

Figure 7 represents the topography of the generated GaN nanofilms on PSi substrate at various wavelengths (1064 nm, 532 nm, and 355 nm) along with three-dimensional AFM images and grain size distribution. Sharp, irregularly shaped particulates are not uniformly distributed across the surface of a GaN film deposited at 1064 nm. The measured surface roughness was 7.62 nm, with an RMS of 2.20 nm. When the laser wavelength was decreased to 532 nm, the GaN film's surface topography altered. As severely angular particles were observed, the surface roughness and RMS increased to 10.64 nm and 3.43 nm, respectively, while oval particles were evenly distributed across the entire surface. When the laser wavelength was decrease to 355 nm, the sharper oval particulates were observed, but not the entire surface, and the surface roughness and RMS increased to 13.62 nm and 6.42 nm, respectively. Table 6 presents the parameters of FM for the Nano-GaN structure grown at different wavelengths of the pulsed laser.

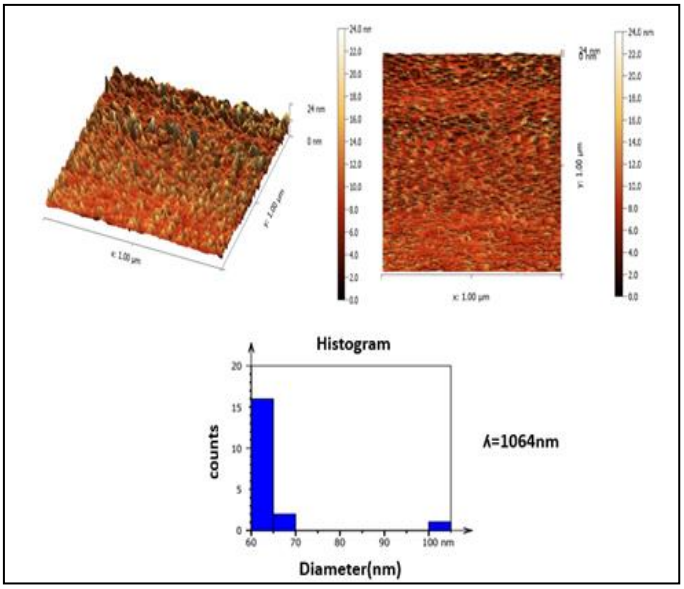

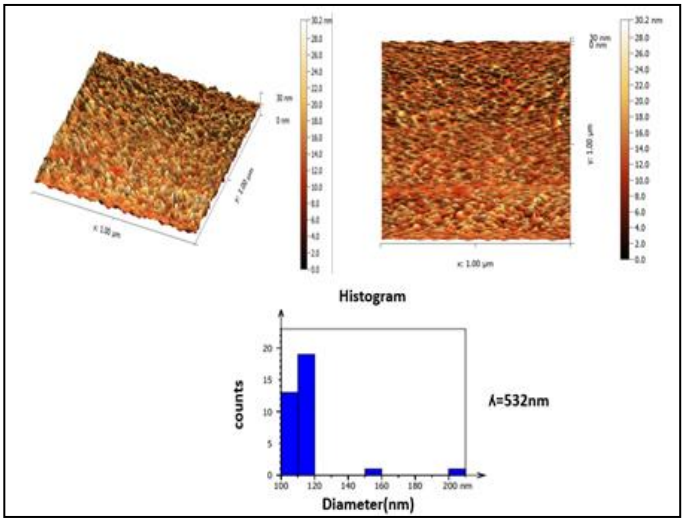

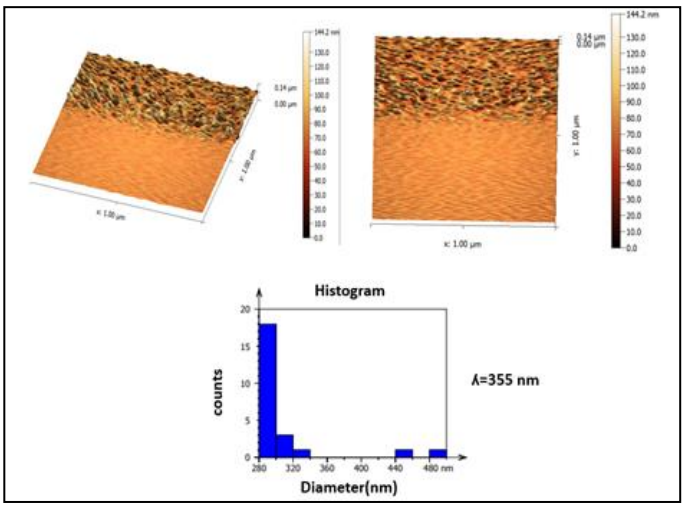

Figure 7. GaN/PSi was produced at various laser wavelengths, producing 3D AFM pictures and particle size dispersion.

Table 6 AFM characteristics for the GaN/PSi fabricated at various laser wavelengths

Wavelengths of pulsed laser (nm)	RMS (nm)	Surface roughness "Average" (nm)
1064	7.62	2.20
532	10.64	3.43
355	13.62	6.42

3.3. The Morphological of the Surface "FESEM"

The surface morphology of porous silicon substrates was examined using FESEM, which revealed the presence of pores with a non-uniform distribution, as shown in Figure 8. The substrate of the PSi has pores of different shapes and sizes morphologically and has an inhomogeneous and nonuniform distribution of pores.

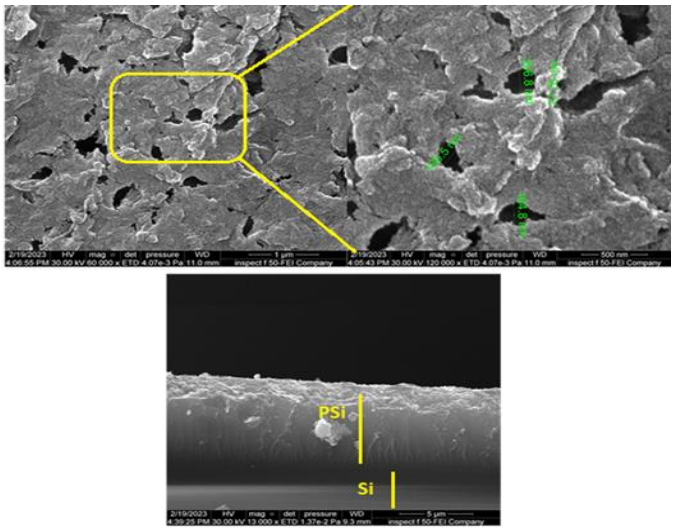

Figure 8. FESEM picture of a PSi substrate that was produced by photo-electrochemical etching with a diode laser.

The surface morphology of GaN films formed on PSi at different wavelengths (1064 nm, 532 nm, and 355 nm) is seen in the FESEM images.The formed GaN film at 1064 nm in Figure.9 A-C shows a smooth and nonhomogeneous distribution of spherical particles on the PSi surface and cross section picture. The FESEM pictures showed particles with a size of 24.51 nm. The GaN layer formed at 532 nm is seen in figures 9 D-F, covering the PSi surface and cross section image with uniform, spherical particles that resemble cauliflowers. At this wavelength the particle size decreased to 23.92 nm. in numbers.9 G-I shows that the Psi surface was covered by the GaN material, which then created nonhomogeneous spherical particles with a cross-section image and morphology resembling cauliflower. The particle size is decreased to 21.30 nm at this wavelength.

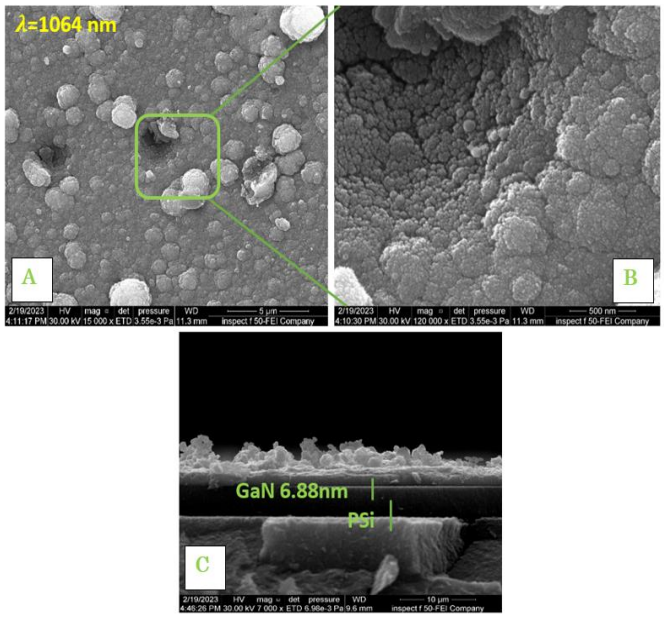

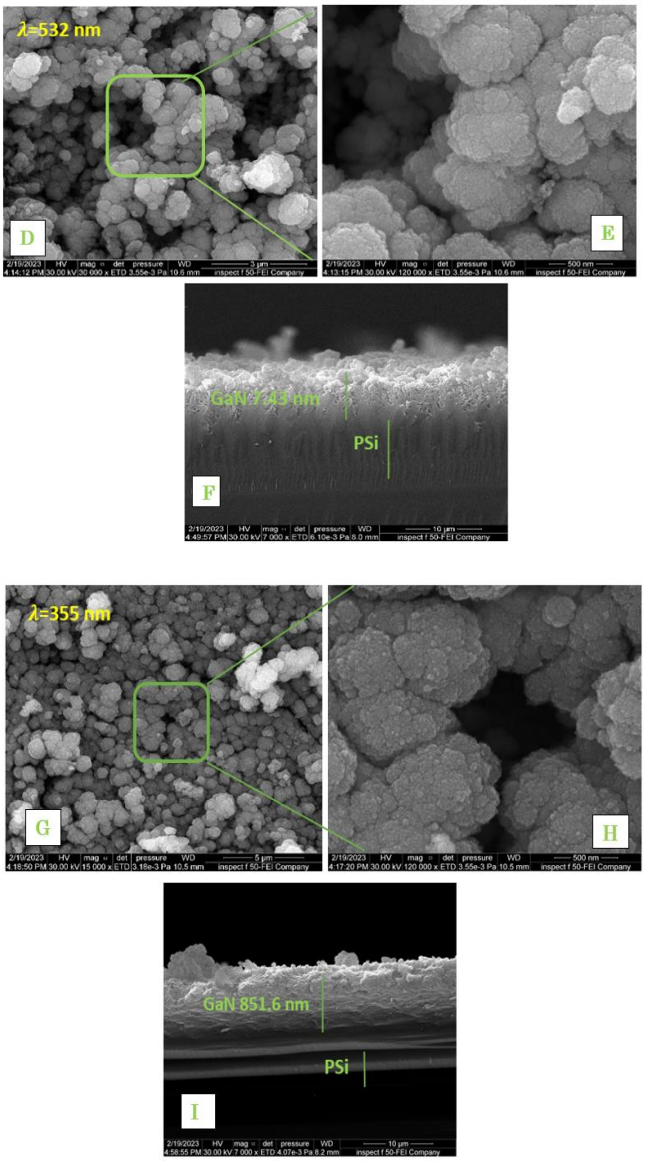

Figure 9. FESEM images of grown GaN film at different wavelength of 1064 nm ,532nm,355 nm and cross section image.

3.4 Energy Dispersive X-ray Spectroscopy (EDX)

Energy Dispersive X-ray Spectroscopy (EDX) is a powerful technique used for analyzing the elemental composition of materials and providing information about the presence and concentration of elements in films. The test EDX spectrum of GaN nanoparticles under various wavelengths (1064 nm, 532 nm, and 355 nm) is displayed in figure 10. It is clear from the figure that there is a high peak of Si, a very small peak of oxygen, and a ratio of [Ga] to [N].

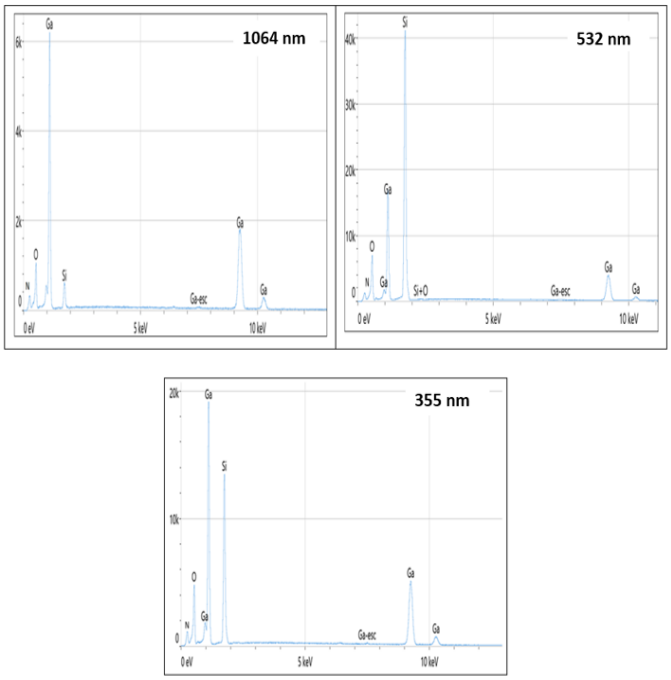

Figure 10. EDX spectrum of the GaN /PSi nano thin film at the wave length 1064, 532, and 355nm.

3.5 Photoluminescence PL results

We performed room-temperature photoluminescence (PL) measurements using a spectrometer covering a wavelength range of 300–900 nm. A red luminescent band with a peak at 810 nm was observed in the PL spectrum of the prepared PSi, as shown in Figure 11. Using Eq. (3), we calculated the energy gap of the PSi sample to be 1.53 eV.

$$E_{gap}=hc/\lambda \quad (3)$$

E_{gap} the optical band gap of the prepared PSi, C the light speed in air (3* 108 m/s), λ wavelength, h for the Planck constant (6.62* 10 -34 J/sec).

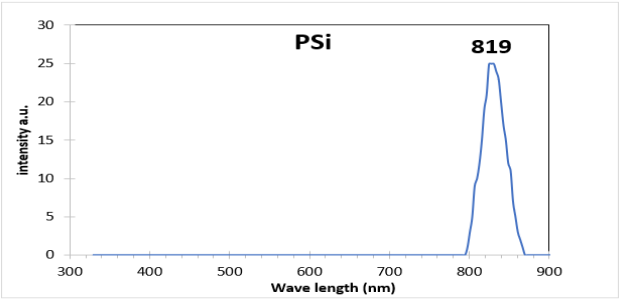

Figure 11. The photoluminescence of a PSi substrate that was prepared using Electrochemical etching induced by laser with the diode laser.

Figure 12 shows the photoluminescence spectra of GaN films produced on PSi substrates, which were examined utilizing laser wavelengths of 1064nm, 532nm, and 355nm. Interestingly, at 1064 nm, a low emission peak of the PL in the bands of UV and an increase in the IR band were detected at an energy gap of 2.88 eV, which can be calculated using Equation (3). A significant high-peak emission of the PL was recorded in the bands of the UV at 532 nm, while there was a drop in the IR band at the energy gap of 3.59 eV. At a wavelength of 355 nm, low emission peaks of the PL in the bands of the UV and an increase in the IR band were seen at an energy gap of 3.00 eV. The same trend was observed with the wavelength's of 1064 nm and 355 nm, indicating that the films possess excellent optical properties across the ultraviolet range.

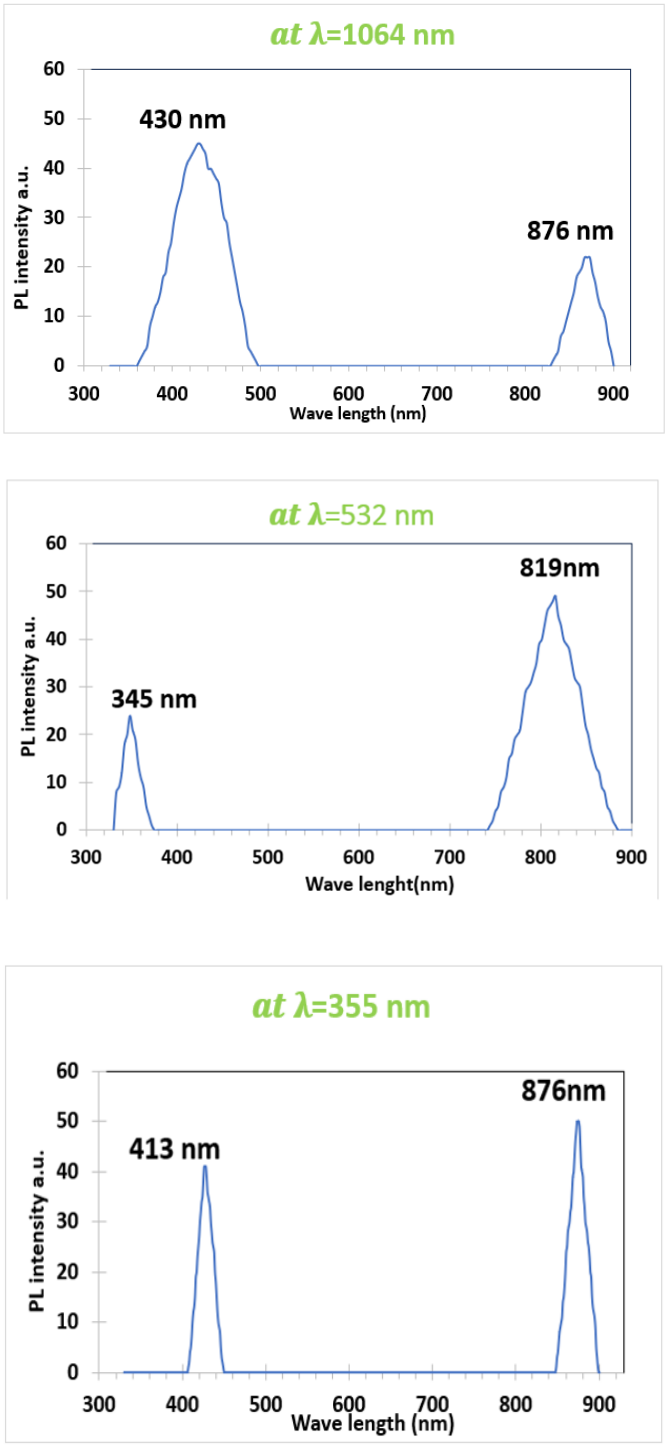

Figure 12. The photoluminescence of GaN/PSi using laser wavelengths of varying values.

3.5. Ultraviolet-Visible Spectroscopy UV

In Figure 13, we present the transmittance of GaN deposition on the quartz with different wavelengths of 1064, 532, and 355 nanometers. We observe that the transmittance rate generally decreases as the wavelength decreases because, when the wavelength decreases, the energy of the photons increases, and as a result, the ablation process on the target increases. This leads to an increase in the deposition rate, which increases the thickness of the membrane and reduces the transmittance. On the other hand, absorption is inversely proportional to transmittance and increases as the wavelength decreases. The band gap values of a GaN thin film are approximately 3.41 eV, 3.46 eV, and 3.49 eV with wavelengths of 1064 nm, 532 nm, and 355 nm, respectively, which was measured via the Tauc plot as shown in Figure 14.

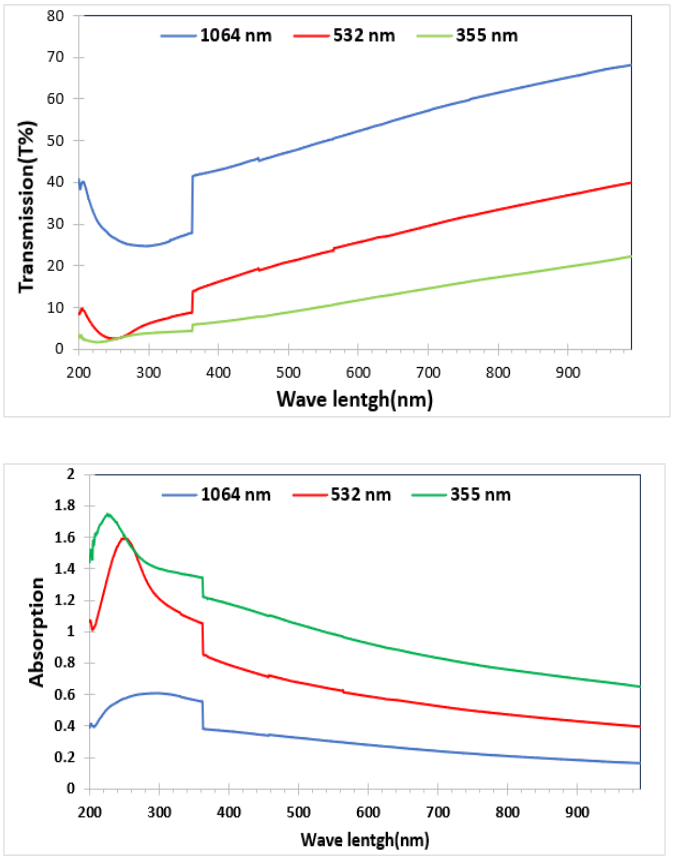

Figure 13. Percentage transmission/absorption versus wavelength of GaN thin film at different wavelength.

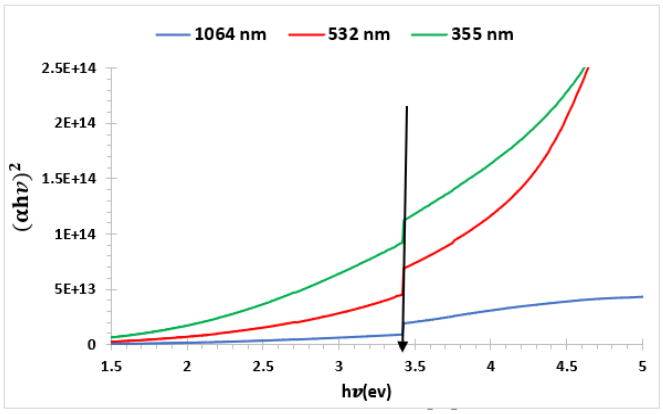

Figure 14. A (hu) against pattern indicating the energy gap.

4. CONCLUSION

In this work, PSi and GaN/PSi samples were prepared using a combination of photochemical etching and pulsed laser deposition (PLD) methods. The Nd:YAG laser's various operating wavelengths (1064, 532, and 355 nm) have been studied to examine these effects on the structure, topography, and spectral characteristics. The findings demonstrated that the produced materials' crystallinity increased as the laser wavelength decreased, and we noted polycrystalline, hexagonal, and cubic structures. According to the spectroscopic analysis's findings, two emission peaks were visible: one in the near-infrared band (at 867, 819, and 876 nm), which was assigned to the PSi substrate, and another in the ultraviolet band (at 430, 345, and 413 nm), which was attributed to the GaN films. Additionally, the energy band gap of the nano-GaN/PSi grew to 3.54 eV as the laser wavelength reached 532 nm. The measurements of the FESEM for the average size of the generated samples revealed that the samples made with the wavelengths of the pulsed laser of 1064, 532, and 355 nm had average diameters of 24.51, 23.92, and 21.30 nm, respectively. The samples exhibited the spherical shapes of the nanoparticles and the like cauliflower shape morphology. Additionally, the AFM tests were used to measure the roughness and root mean square (RMS) values. The results indicated that the sample prepared using a pulsed laser wavelength of 532 nm had the largest roughness, and it also showed complete encapsulation of all PSi-prepared pores. The results showed that the transmission decreased as the wavelength decreased, while the absorption increased with a decrease in the energy gap.

REFERENCES

[1] H. Q. Wu, P. Konkapaka, Y. Makarov, M.G. Spencer, Phys. Stat. Sol. (c) **2**, 2032-2035, (2005).

[2] M. A. Fakhri, E. T. Salim, S. M. Tariq, R. K. Ibrahim, F. H. Alsultany, A. A. Alwahib, S. F. H. Alhasan, S. C. B. Gopinath, Z. T. Salim & U. Hashim, A gold nanoparticles coated unclad single mode fiber-optic sensor based on localized surface plasmon resonance, Scientific Reports, 13, 5680 (2023). https://doi.org/10.1038/s41598-023-32852-6.

[3] A. N. Abd, N. F. Habubi, A. H. Reshak, and H. L. Mansour, Int. J. Nanoelectron. Mater., vol. 11, no. 3, (2018).

[4] T. Zimmermann, M. Neuburger, P. Benkart, F. Hernandez-Guillen, C. Pietzka, M. Kunze, I. Daumiller, A. Dadgar, A. Krost, and E. Kohn, "Piezoelectric GaN sensor structures," IEEE Electron Device Letters, vol. 27, pp. 309-312, 2006.

[5] Salim, E. T., Hassan, A. I., Mohamed, F. A., Wahid, M. H. A., Fakhri, M. A., A sight of view on electrical impacts, structural properties and surface roughness of tungsten trioxide thin film: effect of substrate temperatures in WO3/Si device fabrication, Physica Scripta 2023, 98(3), 035508.

[6] M. A. Fakhri, M. J. A. Razzaq, H. D. Jabbar, E. T. Salim, F. H. Alsultany, U. Hashim, Fabrication of UV photodetector based on GaN/ Psi heterojunction using pulse laser deposition method: Effect of different laser wavelengths, Optical Materialsthis link is disabled, 2023, 137, 113593.

[7] Y. Ikawa, K. Lee, J. Ao, and Y. Ohno, Japanese Journal of Applied Physics, vol. 53, no. 11, 114302, 2014.

[8] Evan T. Salim, Suhair R. Shafeeq, Mohammed Jalal AbdulRazzaq, Makram A. Fakhrib, Subash C. B. Gopinath, Photo-activation of Ag chemicals for enhanced Nb2O5 optoelectronic device employing plasmonic effects, Surfaces and Interfaces, Volume 36, February 2023, 102618.

[9] Fakhri, M. A., Alwahib, A. A., Alhasan, S. F. H., ...Abdulwahab, A. W., Hashim, U., Optoelectronic device based on lithium niobate nanofilms deposited at various pulsed laser wavelengths, Journal of Optics (India) (2023) https://doi.org/10.1007/s12596-023-01173-2.

[10] H. Song, S. Lee, Nanotechnology, vol. 18, no. 25, 255202, 2007.

[11] Osamah, S., Alwahib, A. A., Fakhri, M. A., Gopinath, S. C. B., Study of single and symmetrical D-shaped optical fiber sensor based on gold nanorods, , Journal of Optics (India) (2023)https://doi.org/10.1007/s12596-023-01119-8.

[12] S. Nakamura, Materials Research, vol. 34, pp. 101-107, 2009.

[13] Salim, E. T., Saimon, J. A., Abood, M. K., ...Alsultany, F. H., A Preliminary Study on Structural and Optical Properties of Heat Treated Nb2O5 Nanostructure, International Journal of Nanoelectronics and Materials, 16(1), pp. 21-32 (2023).

[14] Haneen D. Jabbar Makram A. Fakhri, Mohammed Jalal Abdul Razzaq, Omar S. Dahham, Evan T. Salim, Forat H. Alsultany, Effect of Different Etching Time on Fabrication of an Optoelectronic Device Based on GaN/Psi, Journal of Renewable Materials 2023, 11(3), 1101-1122. https://doi.org/10.32604/jrm.2023.023698.

[15] Alwazny, M. S., Ismail, R. A. & Salim, E. T. High-quantum efficiency of Au@LiNbO3 core–shell nano composite as a photodetector by two-step laser ablation in liquid. Appl. Phys. A 128, 500 (2022). https://doi.org/10.1007/s00339-022-05651-5.

[16] Abdulqader D. Faisal, W. K. Kalef, E. T. Salim, F. H. Alsultany, Synthesis of CuO/SnO2 NPs on quartz substrate for temperature sensors application Journal of Ovonic Research Vol. 18, No. 2, March - April 2022, p. 205- 212.

[17] Abdulqader D. Faisal, Wafaa K. Khalef, Evan T. Salim, Forat Hamzah Alsultany, M.H.A. Wahid, Conductivity Modification of ZnO NRs Films via Gold Coating for Temperature Sensor Application, Key Engineering Materials (Volume 936) (2022) 105-114 https://doi.org/10.4028/p-25h5n1.

[18] S. L. Selvaraj, T. Suzue, T. Egawa, IEEE Electron Device Letters, vol. 30, no. 6, pp. 587–589, 2009.

[19] Sara M. Tariq, and Makram A. Fakhri, Design and Simulation of Optical Fibre Based of Gold Nanoparticles for Sensor Applications, International Journal of Nanoelectronics and Materials Volume 15 (Special Issue) December 2022 [59-70].

[20] P. Sai, J. Jorudas, M. Dub, M. Sakowicz, V. Jakštas et al., Applied Physics Letters, vol. 115, no. 18, 183501, 2019.

[21] Rami S. Mohammed, Makram A. Fakhri, Forat H. Alsultany, and U. Hashim, Synthesis of Titanium-Dioxide using Pulsed Laser Deposition at Various Pulsed Laser Energies, International Journal of Nanoelectronics and Materials Volume 15 (Special Issue) December 2022 [93-102].

[22] H. A. A. Abdul Amir, M. A. Fakhri, A. A. Alwahib, E. T. Salim, F. H. Alsultany et al., Sensors and Actuators B: Chemical, vol. 367, 132163, 2022.

[23] Suhair R. Shafeeq, Evan T. Salim, and Mohammed Jalal AbdulRazzaq, Niobium Pentoxide Nanostructures Fabricated by the Fundamental QSwitched Nd:YAG PLD under Vacuum Conditions, International Journal of Nanoelectronics and Materials Volume 15 (Special Issue) December 2022 [1-12].

[24] C. Poblenz, P. Waltereit, S. Rajan, S. Heikman, U. K. Mishra et al., Journal of Vacuum Science & Technology B: Microelectronics and Nanometer Structures Processing, Measurement, and Phenomena, vol. 22, no. 3, pp. 1145–1149, 2004.

[25] Tamara E. Abdulrahman, Rana O. Mahdi, and Evan T. Salim, Synthesis of Nb2O5 Nanoparticle by Liquid Phase Laser Ablation Method, International Journal of Nanoelectronics and Materials Volume 15 (Special Issue) December 2022 [13-25].

[26] Rawan Bashar Fadhil, Evan T. Salim, Wafaa. K. Khalef, and Forat H. Alsultany, Deposition Time Effect on LN Films Properties Using Chemical Bath Deposition Method without Post Heat Treatment, International Journal of Nanoelectronics and Materials Volume 15 (Special Issue) December 2022 [49-58].

[27] S. N. Ogugua, O. M. Ntwaeaborwa, H. C. Swart, Coatings, vol. 10, no. 11, 1078, 2020.

[28] Maryam S. Muhsin, Jehan A. Saimon, and Evan T. Salim, Incorporation of Metal Nanoparticle to Enhance Tungsten Oxide (WO3) Films Properties: A Mini Review, International Journal of Nanoelectronics and Materials Volume 15 (Special Issue) December 2022 [111-118].

[29] Azzam Y. Kudhur, Evan T. Salim, Ilker Kara, Rana O. Mahdi, and Forat H. Alsultany, Applications of Cu2O Nanoparticles Prepared via Various Techniques: A Review Paper, International Journal of Nanoelectronics and Materials Volume 15 (Special Issue) December 2022 [131-137].

[30] A. F. Abdulrahman et al., Nanomaterials, vol. 11, no. 3, p. 677, 2021. DOI: 10.3390/nano11030677.

[31] Fakhri, M.A., Mohammed, R.S., Preparation and characterization of titanium dioxide using PLD at various energy of pulsed laser, Advances in Natural Sciences: Nanoscience and Nanotechnology, 13(4), 045013 (2022). DOI 10.1088/2043-6262/aca60a.

[32] H.D. abbar, M.A. Fakhri, M.J. AbdulRazzaq, Synthesis Gallium Nitride on Porous Silicon Nano-Structure for Optoelectronics Devices. Silicon 14(18), 12837-12853 (2022). https://doi.org/10.1007/s12633-022-01999-8.

[33] A. M. Alia, A. S. Mohammed, and S. M. Hanfooshb, Journal of Ovonic Research, vol. 17, no. 3, pp. 239-245, 2021.

[34] F. A. Mohamed, E. T. Salim, A. I. Hassan, Monoclinic tungsten trioxide (WO3) thin films using spraying pyrolysis: electrical, structural and stoichiometric ratio at different molarity, Digest Journal of Nanomaterials and Biostructures 17(3), 1029 – 1043 (2022).

[35] Rawan B Fafhil, Evan T. Salim, Wafaa. K. Khalef, Synthesis of LiNbO3 microstructures: structural, optical, and surface morphology using Chemical bath deposition (CBD) method without post-heat treatment, Egyptian Journal of Chemistry, 66(4), 63-70 2023, 10.21608/EJCHEM.2022.129669.5749.

[36] E. T. Salim, Surface Review and Letters, vol. 20, no. 5, p. 1350046, 2013. DOI: 10.1142/S0218625X13500467.

[37] Tamara E Abdulrahman, Evan T Salim, Rana O Mahdi and MHA Wahid, Nb2O5 nano and microspheres fabricated by laser ablation, 2022 Adv. Nat. Sci: Nanosci. Nanotechnol. 13 045006 DOI 10.1088/2043-6262/ac99cf.

[38] Evan T. Salim, Ayat Mohammed Yahya, and Ahmed. W. Abdulwahab, Opto-electronic behavior of LN as a dielectric film: Improved using low temperatures treatment, AIP Conference Proceedings 2660, 020130 (2022); https://doi.org/10.1063/5.0107748.

[39] R. Moretta, L. de Stefano, M. Terracciano, and I. Rea, Sensors, vol. 21, no. 4, p. 1336, 2021. DOI: 10.3390/s21041336.

[40] Fakhri M. A., Jabbar H. D., Alsultany F. H., Salim E. T., Hashim U., Lithium Niobate -Based Sensors: A review, AIP Conference Proceedings 2660, 020124 (2022); https://doi.org/10.1063/5.0107759

[41] Rami S. Mohammed and Makram A. Fakhri, Titanium Dioxide -Based Sensors: A review, AIP Conference Proceedings, 2660, 020133 (2022); https://doi.org/10.1063/5.0107767.

[42] J. T. Chen et al Applied Physics Letters, vol. 113, no. 4, p. 041605, 2018. DOI: 10.1063/1.5042049.

[43] Makram A Fakhri, Ali A Alwahib, Evan T Salim, Husam Aldin A Abdul Amir, Forat H Alsultany and U Hashim, Synthesis and characterization of GaN/quartz nanostructure using pulsed laser ablation in liquid Published 19 October Physica Scripta, Volume 97, Number 11 (2022) 115813 DOI 10.1088/1402-4896/ac9866.

[44] H. A. A. A. Amir, M. A.Fakhri, A. A. Alwahib, E. T. Salim, F. H. Alsultany, U. Hashim, Synthesis of gallium nitride nanostructure using pulsed laser ablation in liquid for photoelectric detector, Materials Science in Semiconductor Processing, 150 (2022) 106911.

[45] J. A. Greer, J. Phys. D. Appl. Phys., vol. 47, no. 3, 2014. DOI: 10.1088/0022-3727/47/3/034005.

[46] Evan T. Salim, Ali A. Taha, Sura A. Abdullatef, and Mohammed M. Farhan, Anti-microbial and anti-tumor activity of niobium oxide nano powder, AIP Conference Proceedings 2400, 030015 (2022); https://doi.org/10.1063/5.0112133.

[47] J. Schou, Appl. Surf. Sci., vol. 255, no. 10, pp. 5191-5198, 2009. DOI: 10.1016/j.apsusc.2008.10.101.

[48] M. A. Fakhri et al., "Fabrication of UV photodetector based on GaN/ Psi heterojunction using pulse laser deposition method: Effect of different laser wavelengths," *Opt. Mater. (Amst).*, vol. 137, p. 113593, 2023.

[49] A. Wierzbicka *et al.*, "Arrangement of GaN nanowires on Si(001) substrates studied by X-ray diffraction: Importance of silicon nitride interlayer," *Appl. Surf. Sci.*, vol. 425, no. 001, pp. 1014–1019, 2017, doi: 10.1016/j.apsusc.2017.07.075.

[50] A. F. Wright and J. S. Nelson, "Consistent structural properties for AlN, GaN, and InN," *Phys. Rev. B*, vol. 51, no. 12, p. 7866, 1995.